Oil & Natural Gas Technology

DOE Award No.: DE-FC26-06NT43067

Quarterly Progress Report (July – September 2010)

Mechanisms Leading to Co-Existence of Gas and Hydrate in Ocean Sediments

Submitted by:
Massachusetts Institute of Technology
77 Massachusetts Ave
Cambridge, MA 02139

The University of Texas at Austin
1 University Station C0300
Austin, TX 78712-0228

Prepared for:
United States Department of Energy
National Energy Technology Laboratory

October 30, 2010

Office of Fossil Energy

Executive summary

Work during this period of performance has focused on research activities under Task 7 (Coupled gas/water/sediment dynamics with hydrate formation), in particular Subtask 7.2 (Coupled dynamics with fragile hydrate films).

In previous reporting periods we described our models for gas invasion with hydrate formation. Here, we describe the development of a grain-scale model of hydrate *dissociation*. We concentrate on the process of dissociation from thermal stimulation. Our model incorporates the effects of multiphase flow and sediment mechanics, and we illustrate how these play a role in the dissociation process. Specifically, we study the overpressures generated by dissociation.

Technology transfer activities

During this reporting period, a manuscript has been published in *Phys. Rev. E* on our work on multiphase micromechanics, showing the origin of the crossover from fingering to fracturing in deformable porous media [Holtzman and Juanes, 2010]. The final version of the paper is attached. We are also in the process of finalizing a manuscript on the macroscopic numerical modeling of methane venting from lake sediments [Scandella et al., 2010].

Graduate student Benjamin Scandella and postdoctoral associate Ran Holtzman presented posters at the Gordon Research Conference on Natural Gas Hydrate Systems, which took place at Colby College, Waterville, ME, June 6-10, 2010. Co-PI Ruben Juanes gave one of the plenary invited talks at the same conference, entitled "How methane gas bypasses the hydrate stability zone: observations, mechanisms and models." We have also written three abstracts for presentation at the International Conference on Gas Hydrates in 2011.

Discussion of activities in this reporting period

Task 7: Coupled gas/water/sediment dynamics with hydrate formation; Subtask 7.2: Coupled dynamics with fragile hydrate films

Thermodynamic constraints on overpressure caused by hydrate dissociation

Dissociation of methane hydrate within the pore space of hydrate-bearing sediments (HBS) has often been invoked as a mechanism that may lead to significant overpressures (of up to tens of MPa), in view of the multiple-fold volume increase that would occur upon dissociation [Sultan et al., 2004; Xu and Germanovich, 2006; Kwon et al., 2006]. It has been suggested that such fast pressure buildup could be responsible for massive marine landslides [Sultan et al., 2004; Xu and Germanovich, 2006].

Understanding the pressure evolution within the HBS pore space upon dissociation and the interplay between pore pressure, dissociation rate and sediment mechanics presents a scientifically challenging problem, with crucial implications on the global carbon cycle and energy production. The challenge arises from the strong coupling among the different physical processes: hydrate dissociation increases the gas and water pressures, whereas the driving force for dissociation is proportional to the difference between the equilibrium pressure and the surrounding fluid pressure. In addition, rising pore pressure can deform the sediment matrix and lead to fracture opening, which, in turn, affects the flow properties. The deformation of the sediment and the associated release of methane gas pose a hazard and make it technically difficult to produce gas from both conventional oil and gas reservoirs underlying gas hydrates. Recent studies point out that methane venting can play a significant role in the carbon balance, and, in the arctics, may have a severe impact on the climate [Westbrook et al., 2009; Shakhova et al., 2010].

Previous works conclude that the largest overpressures caused by dissociation by thermal stimulation are expected to occur in fine-grained sediments, where the low permeability inhibits pore pressure dissipation [Xu and Germanovich, 2006; Kwon et al., 2006]. The extreme case of no fluid flow and restricted volumetric expansion was investigated in Kwon et al. [2006]. Since the rising pressure stalls further dissociation, in the absence of pressure dissipation additional heat is required to continue the dissociation process; this "self-preservation" mechanism leads to pressure-temperature (p-T) conditions during dissociation which follow the three-phase (hydrate-gas-brine) equilibrium curve [Kwon et al., 2006]. We stress that this mechanism implies that large overpressures (hereafter defined as the pore pressure above the initial water pressure prior to dissociation) are associated with large temperature increase. For example, the reported overpressure of $\sim$9MPa is associated with a temperature increase of over 9°C, see Fig. 1. We stress that, for such conditions, overpressures of tens of MPa must be accompanied by heating by tens of degrees, which is an unrealistic scenario in many natural and industrial settings.

Here we show that rapid dissociation-induced overpressures are not possible, because an increase in the pore pressure hinders further dissociation. As a result, during the entire dissociation process, the pressure is constrained by the phase equilibrium curve. We investigate the intermediate regime between the two end-members: (1) no-flow (undrained) conditions; and (2) instantaneous pressure dissipation, of fully drained system. We inves-

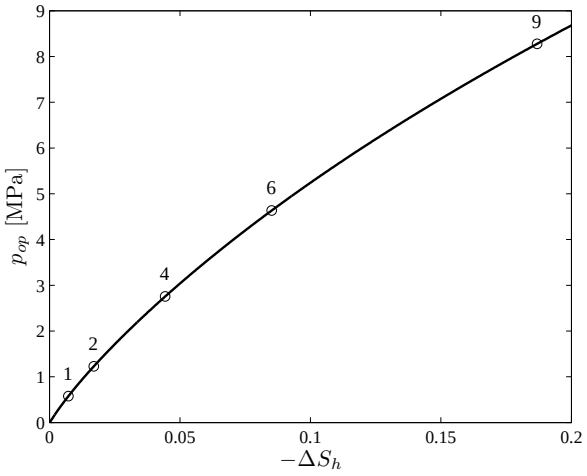

Figure 1: Overpressure p_{op} (pore pressure above the initial water pressure) during thermally-induced dissociation for the extreme case of no fluid flow and restricted sediment volume expansion. The temperature increase required for dissociation to progress is plotted for several hydrate saturation decrements, ΔS_h (positive for saturation increase). The fact that dissociation follows the p-T equilibrium conditions for undrained, volumetrically-restricted conditions, implies that heating by several degrees results in overpressures which cannot exceed several MPa. Computed from Fig. 2 in Kwon et al. [2006].

tigate fine-grained systems (with typical pore size of 1 μm) with different permeabilities (assigning different distributions of pore throat apertures), with partially-drained conditions enforced by reduced (by a factor 10^6) permeability of the outermost pore throats where the pressure outside the sample is held at its value prior to dissociation, p_0. Our results indicate that, because of the coupling between the rate of dissociation and of pressure dissipation, the overpressure is governed by the competition between dissociation and fluid flow.

We present a pore-scale model that couples dissociation kinetics, multiphase flow dynamics and sediment mechanics. We simulate thermally-induced dissociation of a system which is partially saturated with hydrate. Increasing the temperature brings the system out of thermodynamic equilibrium, and hydrate crystals start to dissociate. The conversion of hydrate into water and gas increases the pore pressure, which induces flow. The corresponding fluid pressures depend on the volumes which they occupy. We emphasize the role of drainage by assuming that the driving force for flow is the rise in gas pressure. This pressure is evaluated from an equation of state (EOS), under the assumption that water produced by dissociation takes the volume corresponding to ambient pressure conditions ($\sim$80% of the dissociated hydrate volume for water and hydrate densities of 1 and 0.9 gr/cm^3). We assume that the dissociated gas is nonwetting with respect to the solid mineral grains, initially occupying the interior of the pore body around the dissociating hydrate crystal [Fig. 2(a)]. Once the capillary pressure (gas minus water pressure) exceeds the capillary entry pressure, which is inversely proportional to the pore throat aperture, drainage occurs. Drainage results in gas expansion and thus a drop in gas pressure. In addition, fluid redistribution along the gas-water interface increases the local water pressure, further reducing the capillary pressure [Xu

et al., 2008]. The consequent meniscus adjustments lead to the development a pressure halo around the expanding gas clusters [Fig. 2(b)], exemplifying the non-negligible time required to dissipate water pressure. If gas clusters come in contact, they coalesce into a single cluster (whose pressure is computed by EOS).

We capture the effect of pore pressure on the dissociation by introducing a kinetic model that evaluates the dissociation rate of each hydrate crystal according to the difference between the equilibrium pressure and the surrounding fluid pressure. Additionally, our model incorporates the two-way coupling between fluid displacement and mechanical deformation, providing the mechanisms for pore opening in response to pressure loading (direct coupling), and alteration of the flow properties by grain rearrangements (reverse coupling). The coupling of drainage and sediment deformation is based on the model in Holtzman and Juanes [2010]. Hence, detailed model description is provided for the dissociation kinetics component whereas the coupled flow-deformation model is briefly described. Since the rate of heat dissipation is much faster than that of pressure dissipation, we assume a fixed, uniform temperature, neglecting effects of heat transfer and of the latent heat of dissociation.

A deformable porous media is represented by a 2-D square lattice of dented blocks blocks, connected mechanically by springs [Fig. 2(a)]. The springs are assumed to be prestressed under compression, with sufficiently large confinement to prevent large microstructural rearrangements. The space between the blocks defines the pore volume: the narrow openings between particles are the pore throats, which connect the larger openings (pore bodies). Variation in block shapes leads to disorder in throat apertures, which is assumed to be uncorrelated in space. We construct two interacting networks, a solid network and a fluid network, whose nodes are the solid particles and the pore bodies, respectively. We solve for grain displacements and fluid pressures at the pore bodies.

We model pore-scale disorder by assigning different initial area A and permeability k to the throats between pore bodies. Both the throat area and permeability scale with the square of the throat aperture r, that is, $A \sim r^2$, $k \sim r^2$. We characterize the disorder in throat aperture through a scalar parameter, $\lambda \in (0, 1)$, drawing aperture values from a uniform distribution, $r \in [1-\lambda, 1+\lambda]\bar{r}$, where $\bar{r} \sim a$. The characteristic length scale is the pore size a, which here we take as half the distance between nodes in the lattice.

We assume that gas is nonwetting with respect to the solid grains, and inviscid. Hence, gas pressure adjusts instantaneously upon dissociation and drainage. The pressure at each gas cluster is computed from its volume and the number of moles through an EOS. For simplicity, we use here the ideal gas law; usage of a more accurate EOS is straight-forward.

The water pressure in an undrained pore is evaluated from mass conservation at a pore body: $p(t+\Delta t) = p(t) + \sum_j q_j \Delta t/(c_t V)$, where Δt is the time step, V is the pore volume, and the summation is over all neighboring pores. The volumetric flow rate between the pore and its neighbor j is given by Darcy's law $q_j = (Ak/\mu)(p_j - p)/\ell_j$, where μ is the water dynamic viscosity and ℓ_j is the length over which the pressure drop $p_j - p$ is applied. For flow between two undrained pores, $\ell = 2a$. If pore j is drained, the meniscus between the two pores starts advancing if the capillary pressure exceeds the capillary entry pressure, $p_j - p > 2\gamma/r$, where γ is the gas-water interfacial tension. The length over which viscous pressure drop takes place decreases as the meniscus advances, according to the expression $\ell_j(t + \Delta t) = \ell_j(t) - (q_j/A)\Delta t$. The consequent pressure variations in the undrained pore are governed by the ability of the medium to dissipate pressure through the effective compressibility c_t. An

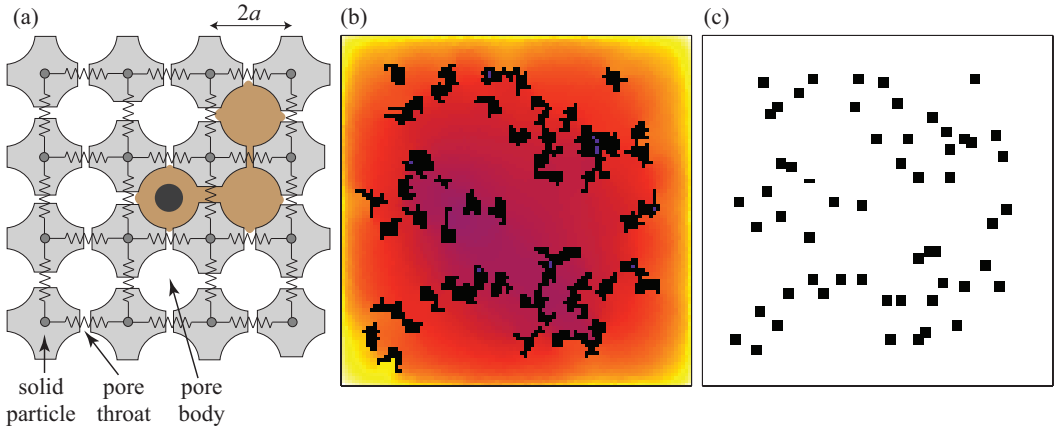

Figure 2: (a) Schematic of the model. The solid matrix is represented by a square lattice of dented blocks, connected mechanically by springs. The narrow openings between particles are the pore throats, which connect the larger openings (pore bodies). Some of the pore bodies are initially filled with a hydrate crystal (marked by black disc). Dissociation converts portions of the hydrate mass into water (white) and free gas (brown). (b) Pore pressure during simulation of dissociation. The color scheme represents the logarithm of pressure normalized by the average gas pressure. Black represents drained pores filled with gas, and, in some cases, with hydrate crystals [position shown in (c)]. White corresponds to the ambient water pressure (prior to dissociation). The pressure halo that surrounds the interior gas clusters reflects the finite timescale required for water pressure dissipation. The coalescence of the growing gas clusters [originally contained in the pore space around hydrate crystals, see (c)] is necessary for establishing gas flow across the sample, and gas production.

effective compressibility $c_t = a/\gamma$ is assigned to the nearly-incompressible water to represent the fluid redistribution along the meniscus [Holtzman and Juanes, 2010].

Grain rearrangements cause changes in the contraction of the springs over time, $h(t)$. To highlight the effect of disorder in flow properties, we assume the system is initially pre-stressed homogeneously, such that all springs are subject to the same compression, h_0, corresponding to a macroscopic strain $\epsilon_0 = h_0/2a$. Each grain is subject to two types of forces: pressure forces and contact forces. The force exerted on a grain by the fluid occupying an adjacent pore body is oriented at 45° and is of magnitude $f_p = pA_p$, where $A_p \sim a^2$ represents the area upon which the pressure acts. The intergranular contact forces f_c are updated by $f_c(t + \Delta t) = f_c(t) + K\Delta h$, where K is the spring stiffness and $\Delta h = h(t + \Delta t) - h(t)$ is the change in spring contraction. Grain positions are determined at the new time step by imposing force balance at every block, $\sum(\vec{f_p} + \vec{f_c}) = \vec{0}$, which leads to a linear system of equations to be solved for Δh of every spring. Grain displacements impact fluid flow because they modify the throat apertures. We evaluate changes in throat apertures and in intergranular forces from the grain displacements in analogy with cubic packing of particles with frictionless, Hertzian contacts, such that $\Delta r = -\Delta h(1 - \epsilon)/[2\sqrt{1 + (1 - \epsilon)^2}]$, where $\epsilon = h(t)/2a$, and the spring stiffness $K = 2E^*\sqrt{R^*h}$, where $R^* = a/2$, and E^* is the constrained Young modulus of the grain material Johnson [1987]. We model an unconsolidated sediment with negligible tensile strength. Therefore, a spring is removed when there is net elongation between blocks ($h \leq 0$). A small cohesive force is applied as a regularization parameter. This force is orders of magnitude smaller than the typical pressure force, and we have confirmed that the results are insensitive to the value of this cohesive force, as long as it is small.

The mass of hydrate dissociated at each time step Δm_h is determined according to a kinetic rate which is proportional to the difference between the three-phase equilibrium fugacity f_e and the methane fugacity at the hydrate crystal surface f [Kim et al., 1987]

$$\Delta m_h = -K_0 \exp(\frac{-E}{RT}) F_A A_h (f_e - f)\Delta t. \tag{1}$$

where K_0 is the hydration reaction constant, E is the hydration activation energy, A_h is the surface area for the reaction (computed from its volume assuming spherical crystal, using $F_A = 1$ for the area adjustment factor), and R is the universal gas constant. We evaluate f_e and f from the equilibrium pressure (for temperature T) and the pressure of gas surrounding the dissociating crystal. Negative value of Δm_h means decrease in hydrate mass. The dissociated hydrate volume $\Delta V_h = \Delta m_h/\rho_h$ is partially replaced by water (∼80% at $p_w = p_0$), where the remainder volume is taken by gas. We use hydration number of $N_h = 5.75$ [Max, 2003] in determining the produced mass of water and methane, with densities of $\rho_h = 0.9$ gr/cm^3 and $\rho_h = 1$ gr/cm^3.

Our results indicate that the timescale of pore pressure increase by dissociation t_d is greatly exceeds that of pressure dissipation t_p, associated with gas expansion by drainage of one or more pore and dissipation of the water pressure ahead of the moving meniscus [Fig. 3]. We stress that the rapid pore pressure dissipation restricts the pore pressure, and that the pressure remains below the equilibrium value p_{eq} since their equality implies diminishing driving force for further dissociation and gas generation. Note that, if the pressure at some part of the sample rises above p_{eq}, for instance due to dissociation in a remote location, the

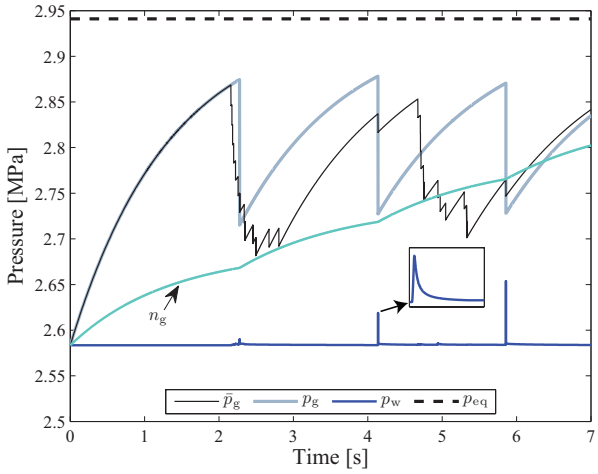

Figure 3: Typical pressure evolution during simulation of thermally-stimulated hydrate dissociation. The equilibrium pressure p_{eq} is shown in dashed line. The pressures in a gas p_g and a nearby water p_w pore are shown in gray and blue, respectively. The decreasing dissociation rate due to the increasing methane pressure [reducing the driving force for dissociation, see Eq. (1)] is clearly shown in the concave shape of both the gas pressure and the number of gas moles within that cluster (n_g, normalized quantity plotted in green). Once the gas pressure exceeds the sum of the capillary entry pressure and the water pressure in an adjacent undrained pore, drainage occurs (marked by sharp drop in gas pressure). The timescale for the recovery of gas pressure $t_{\rm d}$ (few seconds) is 5–6 orders of magnitude larger than that of pore pressure dissipation $t_{\rm p}$; the time for water pressure dissipation following an invasion event (inset) is $\sim 10^{-5}$s. The volume-averaged gas pressure $\bar{p}_g = \sum_j (p_j V_j) / \sum_j V_j$ (summation over all drained pores, marked by black solid line) captures the multiple invasion events within the different gas clusters. In all the simulations (unless stated otherwise) we use network of 100×100 pores with $\lambda = 0.2$, and set $a = 1$ μm, $\mu = 10^{-3}$ Pa$\cdot$s, $\gamma = 0.07$ N m^{-1}, and $\epsilon_0 = 0.01$. In Eq. (1) we use $F_A = 1$, $R = 8.314$ J mol^{-1} K^{-1}, $E = 8.1 \cdot 10^4$ J mol^{-1}, and $K_0 = 3.6 \cdot 10^4$ Kg m^{-2} Pa^{-1} s^{-1}. Here, the initial temperature and pressure conditions are $T_0 = 0.5$°C (273.65K) and $p_0 = 2.58$MPa, with applied heating by $\Delta T = 1.55$°C.

reversible nature of hydrate dissociation can lead to hydrate reformation at the pressurized location [Moridis et al., 2005]. Hydrate reformation is not currently included in the model, though it can be easily introduced, for instance by allowing the value of Δm_h in Eq. (1) to become positive.

The contrast in timescales can be deduced by scaling: the pressure dissipation timescale is $t_{\rm p} \sim L_{\rm p}^2/D$, where $D = (k/\mu)/c_t$ is the hydraulic diffusivity, and $L_{\rm p}$ a is the length over which the pressure dissipation takes place. With $k \sim a^2$ and $c_t \sim a/\gamma$ we obtain $t_{\rm p} \sim \mu L_{\rm p}^2/(\gamma a)$. The dissociation timescale is obtained from Eq. (1) by using the EOS to replace Δm_h with the corresponding gas pressure increment, and assuming it is of similar order of magnitude as the fugacity driving force $f_e - f$. This provides $t_{\rm d} \sim (M_h a)/(RTK_0 \exp(\frac{-E}{RT}))$. Using published values of $E = 8.1 \cdot 10^4$ J mol^{-1} and $K_0 = 3.6 \cdot 10^4$ Kg m^{-2} Pa^{-1} s^{-1} [Kim et al., 1987; Clark and Bishnoi, 2001; Moridis et al., 2005], where $M_h = 0.119$ gr mol^{-1} is the molar

mass of hydrate (for $N_h = 5.75$), and with $a = 1$ μm, $\mu = 10^{-3}$ Pa $\cdot$ s and $\gamma = 0.07$ N m^{-1} results in more than 5 orders of magnitude (depending on the scaling used for $L_{\rm p}$; using $L_{\rm p} \sim a$ results in 8 orders of magnitude difference).

The rapid pressure dissipation by drainage implies that the overpressure is determined by the typical capillary pressures p_c^e: once the gas pressure reaches p_c^e it will expand by invasion and its pressure will be reduced. The overpressures above the initial water pressure p_0 are typically bound by the capillary entry pressures [Fig. 4]. We note that the overpressures are always below the equilibrium pressure $p_{\rm eq}(T)$; once the gas pressure reaches that value dissociation will stop with no further heating. The maximum overpressure, measured as the maximum value reached by $\bar{p}_g$ above p_0 during the entire simulation for systems with different pore-scale permeability $k = \bar{r}^2$. In these simulations, the typical throat aperture is determined by multiplying the value predicted from the assumed cubic packing geometry $\bar{r}_{\rm geom} = a[\sqrt{1 + (1-\epsilon)^2} - 1]$ by a throat-to-pore size adjustment factor, $\beta = \bar{r}/\bar{r}_{\rm geom}$. This allows to vary $\bar{r}$ independently of a (keeping $a = 1$ μm in all the simulations). The value of β in Fig. 4 ranges from 1/2 (increase by factor of 2 relative to the expected value from geometry) to 50. The amount of heating ΔT applied was 0.5°C on top of the value required for complete dissociation, where the dependance of the latter on $\bar{r}$ is reflected by the increasing ΔT value applied (1.0–18.8°C). While for most of the simulations the overpressures are bound between the minimum and maximum capillary entry pressure values, $p^e_{\rm c,\ min} = 2\gamma/(1+\lambda)$ and $p^e_{\rm c,\ max} = 2\gamma/(1-\lambda)$, the tendency towards the maximum entry pressure $p^e_{\rm c,\ max}$ increases with increasing k. This is due to heterogeneity: the expanding gas invades more pores in the higher-permeability systems, hence sampling a larger portion of the pores in the sample. The higher capillary pressure in tighter samples with lower k reduces the final gas saturation (once dissociation is completed), implying that only pores with the widest throats are invaded. Finally, for sufficiently deformable medium, in which the capillary pressure is large enough to deform the solid skeleton given its stiffness and the confining stress, grain rearrangements lead to fracturing by opening some of the pore throats and forming a highly-preferential flow path [Holtzman and Juanes, 2010]. Fracturing occurs at value of capillary pressures which are lower than the entry pressures in the original (undeformed) system. This mechanism explains the deviation below the maximum entry pressure values for low-permeability samples.

To verify that our results hold for a wide range of conditions, we also conducted simulations using larger values of K_0. While the timescale of dissociation becomes proportionally smaller, and, in theory, can become equivalent to that of pressure dissipation, the overpressures never exceed the equilibrium pressure.

In conclusion, we have shown that regardless of the kinetic rate of dissociation, heat supply, and sediment permeability, the overpressure is bounded by the pressure at thermodynamic equilibrium. Moreover, we find that for kinetic rates suggested in the literature the timescale of dissociation is much larger than that of pressure dissipation, further restricting the maximum possible overpressure. These findings bear important consequence for the response of natural sediments to ocean warming, and for future methane production from HBS. Economically-recoverable production technology depends both on the produced rates, as well on geohazards associated with formation damage and fracturing. Pore pressure evolution and the corresponding changes in the flow and mechanical properties are key in understanding the impact of dissociation in hydrate-bearing sediments.

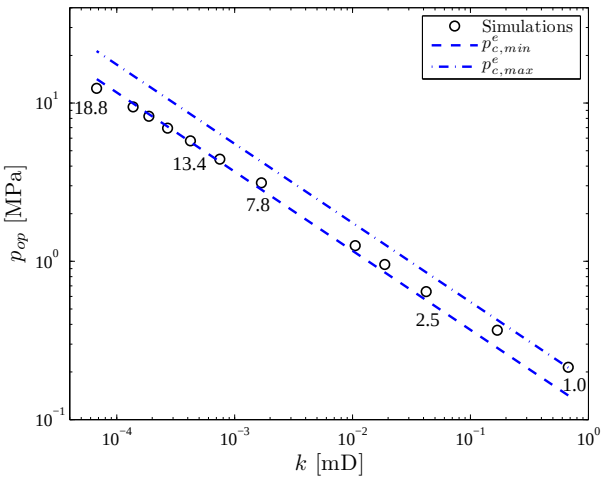

Figure 4: The maximum overpressure $p_{\rm op} = \bar{p}_g - p_0$ reached during the simulations for systems with different permeability, $k = \bar{r}^2$. The typical throat aperture $\bar{r}$ is varied using different throat-to-pore ratio, keeping $a = 1$ μm in all the simulations. The amount of heating ΔT (in °C) applied, 0.5°C above the value required for complete dissociation, is printed for some of the simulation. Since the timescale for pore pressure buildup by dissociation is much larger than that for pressure dissipation by drainage, $t_{\rm d} \gg t_{\rm p}$, in most simulations the overpressures are bounded between the minimum and maximum capillary entry pressure values, $p^e_{\rm c,\ min} = 2\gamma/(1+\lambda)$ and $p^e_{\rm c,\ max} = 2\gamma/(1-\lambda)$ (here, $\lambda = 0.2$). Note that the equilibrium pressure $p_{\rm eq}(T)$ is, by definition, larger than $p^e_{\rm c,\ max}$ (otherwise complete dissociation is not possible, due to the lack of driving force). In low-permeability samples, the high capillary pressures suffice to overcome confining stress given the solid skeleton stiffness, prior to invasion by capillarity (overcoming $p^e_{\rm c}$). Fracturing by grain rearrangements reduces the capillary pressure required for invasion [Holtzman and Juanes, 2010], a mechanism responsible for the deviation of $p_{\rm op}$ below the $p^e_{\rm c,\ min}$ line. The tendency of the overpressure for systems with high k values to reach the upper limit of entry pressures $p^e_{\rm c,\ max}$ is due to heterogeneity: the expanding gas invades more pores in the high-permeability systems, hence sampling a larger portion of the pores in the sample. The higher capillary pressure in tighter samples with lower k reduces the gas saturation after dissociation is completed, so that most of the invasion is occurring through the widest throats.

References

M. Clark and P. R. Bishnoi. Determination of activation energy and intrinsic rate constant of methane gas hydrate decomposition. *Can. J. Chem. Eng.*, 79(1):143–147, doi=10.1002/cjce.5450790122, 2001.

R. Holtzman and R. Juanes. Crossover from fingering to fracturing in deformable disordered media. *Phys. Rev. E*, 82:046305 (2010), doi:10.1103/PhysRevE.82.046305, 2010.

K. L. Johnson. *Contact Mechanics*. Cambridge University Press, 1987.

H. C. Kim, P. R. Bishnoi, R. A. Heideman, and S. S. H. Rizvi. Kinetics of methane hydrate decomposition. 42(7):1645–1653, doi=10.1016/0009–2509(87)80169–0, 1987.

T. H. Kwon, G.-C. Cho, and J. C. Santamarina. Gas hydrate dissociation in sediments: Pressure-temperature evolution. *Geochem. Geophys. Geosyst.*, 9(3):Q03019, doi=10.1029/2007GC001920, 2006.

M. D. Max, editor. Kluwer, Dordrecht, The Netherlands, 2003.

G. J. Moridis, Y. Seol, and T. J. Kneafsey. Studies of reaction kinetics of methane hydrate dissociation in porous media. In *Proc. Fifth Intl. Conf. Gas Hydrates*, Trondheim, Norway, 2005.

B. P. Scandella, C. Varadharajan, H. Hemond, C. Ruppel, and R. Juanes. Methane venting from lake sediments. 2010. (In preparation).

N. Shakhova, I. Semiletov, A. Salyuk, V. Yusupov, D. Kosmach, and Ö. Gustafsson. Extensive methane venting to the atmosphere from sediments of the East Siberian Arctic shelf. *Science*, 327:1246–1250, 2010.

N. Sultan, P. Cochonat, J.-P. Foucher, and J. Mienert. Effect of gas hydrates melting on seafloor slope instability. *Mar. Geol.*, 213:379–401, 2004.

G. K. Westbrook, K. E. Thatcher, et al. Escape of methane gas from the seabed along the West Spitsbergen continental margin. *Geophys. Res. Lett.*, 36:L15608, doi:10.1029/2009GL039191, 2009.

L. Xu, S. Davies, A. B. Schofield, and D. A. Weitz. Dynamics of drying in 3D porous media. *Phys. Rev. Lett.*, 101:094502, 2008.

W. Xu and L. N. Germanovich. Excess pore pressure resulting from methane hydrate dissociation in marine sediments: A theoretical approach. *J. Geophys. Res.*, 111:B01104, doi:10.1029/2004JB003600, 2006.

National Energy Technology Laboratory

626 Cochrans Mill Road
P.O. Box 10940
Pittsburgh, PA 15236-0940

3610 Collins Ferry Road
P.O. Box 880
Morgantown, WV 26507-0880

One West Third Street, Suite 1400
Tulsa, OK 74103-3519

1450 Queen Avenue SW
Albany, OR 97321-2198

2175 University Ave. South
Suite 201
Fairbanks, AK 99709

Visit the NETL website at:
www.netl.doe.gov

Customer Service:
1-800-553-7681